Scaling rules for diffusive drug delivery in tumor and normal tissues

James W. Baish[a,1], Triantafyllos Stylianopoulos[b], Ryan M. Lanning[b], Walid S. Kamoun[b], Dai Fukumura[b], Lance L. Munn[b], and Rakesh K. Jain[b,1]

[a]Departments of Mechanical and Biomedical Engineering, Bucknell University, Lewisburg, PA 17837; and [b]Edwin L. Steele Laboratory for Tumor Biology, Massachusetts General Hospital and Harvard Medical School, Boston, MA 02114

Delivery of blood-borne molecules and nanoparticles from the vasculature to cells in the tissue differs dramatically between tumor and normal tissues due to differences in their vascular architectures. Here we show that two simple measures of vascular geometry—δ_{max} and λ—readily obtained from vascular images, capture these differences and link vascular structure to delivery in both tissue types. The longest time needed to bring materials to their destination scales with the square of δ_{max}, the maximum distance in the tissue from the nearest blood vessel, whereas λ, a measure of the shape of the spaces between vessels, determines the rate of delivery for shorter times. Our results are useful for evaluating how new therapeutic agents that inhibit or stimulate vascular growth alter the functional efficiency of the vasculature and more broadly for analysis of diffusion in irregularly shaped domains.

antiangiogenesis | cancer | fractal dimension | percolation | transport

Blood vessels in tumors are highly irregular compared to those in normal tissues (Fig. 1). Unlike normal vessels, tumor vessels lack an orderly branching hierarchy from large vessels into successively smaller vessels that feed a regularly spaced capillary bed. Instead, tumor vessels are dilated, tortuous, and leaky and leave unperfused regions of many sizes (1, 2). Here we address the question of how such differences affect the delivery of blood-borne agents such as nutrients, drugs, and imaging tracers—essentially how much material entering the arterial supply reaches a given location in the tissue and how long it takes to get there. Numerous studies of normal tissues have exploited the orderly branching patterns of the arterial network and the highly regular spacing of the capillary bed to devise powerful mathematical relationships linking the typical spacing between blood vessels to their ability to carry out their transport function (3–5). Unfortunately, analogous relationships in tumors have been more elusive due to their more chaotic vascular architectures that lack an obvious length scale, such as the intercapillary spacing, upon which a model can be built. Here we show that despite the differences between tumor and normal vasculature, simple scaling rules can be deduced that relate the number and spacing of blood vessels to the quantity of material transported from arterial supply to cell in a given time.

Transport from a feeding artery to a cell in the tissue is a two-step process. First, materials flow near to their destination via blood vessels. Then they cover the remaining distance from the blood vessels to the cells via diffusion and convection. In the case of solid tumors, convection is negligible everywhere except at the tumor margins (6). The time required for diffusion over large distances is often much longer than that needed for flow, because diffusion times grow as the square of distance whereas flow times are proportional to distance. Under normal conditions, blood is distributed to the capillary bed through an orderly tree-like system of conduits. From there, normal diffusion distances are highly regulated, generally to less than 50 or 100 μm, so that no cells exceed the distance that oxygen and other nutrients can diffuse before being metabolized (7). To develop a more general set

of scaling rules for tumors and normal tissues, we must account for the highly variable diffusion distances from vessel to cell.

Results

Tracer Clearance Studies Provide Insight into Diffusive vs. Convective Transport. We first examined our previously reported results from a tracer clearance study in animal tumors of about 1 mL volume with the goal of linking them to the vascular architecture (Fig. 2) (8). We isolated the effects of flow from those of diffusion by injecting pulses of two different, nonspecific tracers into the same organ: one that by virtue of its large molecular weight cannot pass through the blood vessel walls, and another of smaller molecular weight that diffuses freely through the vessel walls. We found that the diffusible tracer cleared more slowly from a tumor than an intravascular tracer and that both tracers showed greater dispersion of transit times in tumors than reported for a diffusible tracer in a highly vascular, normal tissue—the myocardium (9).

How do we interpret these results? The time required for a large molecule to traverse the organ depends only on the time required to flow from inlet to outlet along its route within the vasculature, whereas small molecules can flow part way, then diffuse out of and back into a vessel one or more times, and finally exit the tissue within the flow. A rapid rise and fall in outlet concentration indicates that all tracer molecules experience relatively similar paths, whereas a more gradual decay suggests that flow and diffusion times are more heterogeneous throughout the tissue. The relatively rapid decay observed for a diffusible tracer in normal tissue indicates that, compared to the tumors, all flow paths are similar and the distances over which extravascular diffusion takes place are relatively short. In contrast, we see the more gradual clearance of an intravascular tracer from tumors as evidence that blood flow heterogeneity, while present in all tissues, is more pronounced in tumors than in normal tissues. In tumors there is little correlation between blood flow velocities and vessel diameters (10, 11). Moreover, tumors are known to contain arteriovenous shunts that serve as pathways of low-flow resistance and high velocity as well as a multitude of secondary pathways that carry slower-moving blood (12). As a result, the concentration of tracer in tumor vasculature may be expected to vary with location and time as seen in the wider range of transit times for intravascular tracers in tumors than for diffusible tracers
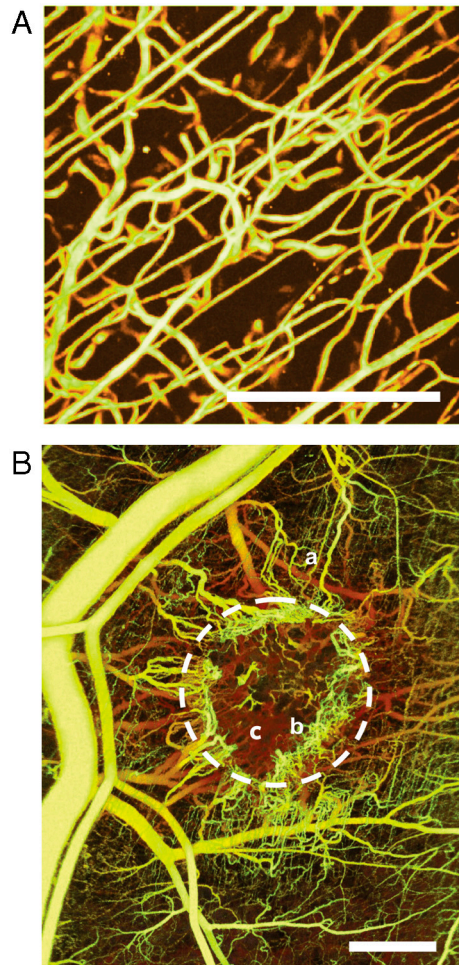
ENGINEERING

MEDICAL SCIENCES

Fig. 1. Vasculature in normal subcutaneous and tumor tissues. (*A*) Normal capillaries appear as fine, nearly parallel vessels that are served by orderly, branching arterial, and venous trees (26) (Scale bar = 100 μm). (*B*) A mammary carcinoma (MCaIV) was grown in mammary fat pad of a mouse using a procedure described in (27) and imaged with Doppler optical frequency domain imaging (28) (Scale bar = 1 mm). Growth factors secreted by the tumor promote dilation and tortuosity of the capillaries (a) outside the tumor margin (dashed line). In contrast, the tumor vessels are highly disorganized (b), leaving large, irregular avascular spaces (c).

Fig. 2. Tracer clearance from vascular networks. Venous output concentrations were measured following a brief arterial injection into breast tumor that was grown in a rat with a single arterial supply and venous return by a procedure described in Eskey et al. (8). Output concentrations are shown for two blood-borne agents—one intravascularly restricted due to its large molecular weight (IVT), the other free to diffuse from the vasculature to the adjacent tissue (D_2O). Due to the short duration of the input, at long-times the output concentration approximates the residence time from a perfect pulse $h(t)$. A typical trial is shown in which the tails of the outputs are fit to power laws: $h_{D_2O}(t) \sim t^{-1.67}$ and $h_{IVT}(t) \sim t^{-2.36}$. Averaging 2 trials on each of 4 tumors we find $h_{D_2O}(t) \sim t^{-1.73\pm0.09}$ and $h_{IVT}(t) \sim t^{-2.29\pm0.20}$ with a tumor mass of $m = 1.06 \pm 0.17$ *g* (mean ± SEM). For comparison, published results (9) for a highly diffusible tracer (O^{15}) in normal myocardium yielded a narrower range of transit times ($h_{O^{15}}(t) \sim t^{-3.1}$).

in normal tissue ($t^{-2.29\pm0.20}$ vs. $t^{-3.1}$). The still slower clearance of a diffusible tracer in tumors is a sign that large diffusion distances exist in tumors ($t^{-1.73\pm0.09}$ vs. $t^{-2.29\pm0.20}$). The long-time tail of the clearance arises from those parts of the tissue to which delivery of nutrients and therapeutic drugs is most difficult—potentially a significant fraction of the total tissue volume.

When the voids between vessels are sufficiently large, extravascular diffusion can take so long that the concentration in the well-perfused vessels becomes relatively uniform as evidenced by the divergence at long times of the clearance curves for diffusive molecules from those of intravascular tracers. We provide analysis (*SI Discussion, Analytical Model of Diffusion*) and simulations (*SI Discussion, Numerical Simulations for Specific Geometries*) that further demonstrate how diffusion can dominate the clearance process even when significant flow heterogeneity is present. This allows us to create computational models of extravascular diffusion from high-resolution 3D images such as those in Fig. 1 even though these images do not contain explicit information on the blood flow rates.

Computational Models of Diffusion Based on High-Resolution Images. We create such models by assuming that the tracer satisfies the

three-dimensional time-dependent diffusion equation in the space exterior to the blood vessels. The boundary condition is a prescribed concentration at the vessel walls, and the initial condition is a (different) uniform concentration throughout the tissue space. For measured vascular network geometries, this equation is solved approximately using a random-walk simulation. Details are provided in the caption to Fig. 3. We show (*SI Discussion, Analytical Model of Diffusion*) how these results can be related to the tracer clearance experiments considered earlier and other relevant pharmacokinetic measures such as the half-life, peak concentration, and the area under the time-concentration curve.

Fig. 3*B* shows results from random walks typical of those from normal and tumor tissues. We note two features that deserve a physical explanation relative to the vascular geometry: a transition to exponential decay at long times (e^{-t/t_c}), where t_c is the time constant, and an earlier interval characterized by an approximate power law ($t^{-\alpha}$) with a drifting exponent α that differs somewhat from the value 1/2 usually associated with diffusion processes at short times. Recognizing that short times correspond to short distances from the vessels and long times to long distances we hypothesize that the rates of clearance should be related to how much of the tissue resides at a given distance from the nearest blood vessel.

To further investigate how the time dependence of our results depends on the geometry of the vasculature, we consider histograms of the number of voxels at a given distance from the nearest vessel $n(\delta)$ as obtained from 3D images such as those in Fig. 1 (Fig. 3*C*). These statistics can be readily compiled and many have been published (13). We note that $n(\delta)$ for normal tissues rises to a peak and then drops quickly as the maximum distance from a vessel is approached. In contrast, $n(\delta)$ in a typical tumor drops more slowly toward a much larger maximum distance indicating that diffusion times and the transition to exponential decay are much longer than in normal tissue. We find that the time constants obtained from best fits on the long-time behavior of our random walks on vascular images correlate strongly with the maximum distance to the nearest vessel δ_{max}, averaging $t_c \approx 0.43\delta_{max}^2/D_m$ where D_m is the molecular diffusivity. In principle, the constant of proportionality can depend weakly on the
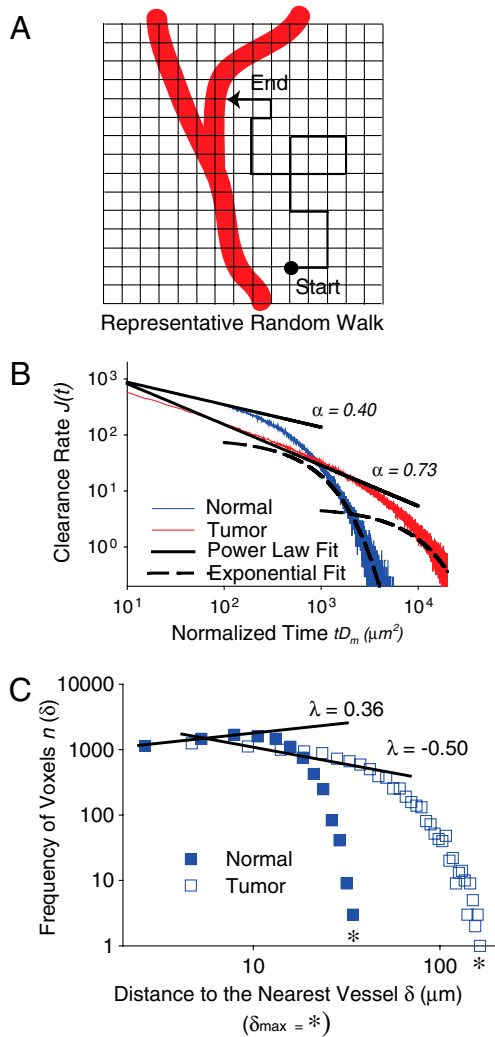
Fig. 3. Diffusion in the extravascular tissue of normal and tumor tissue. 3-D images of the transparent window ($600 \times 600 \times 150$ voxels) similar to those in Fig. 1 were obtained using Doppler optical frequency domain imaging for normal capillaries and a mammary carcinoma MCaIV (*SI Materials and Methods*). (*A*) Extravascular diffusion was simulated by random walks of 10^6 walkers, released at random voxels in the extravascular space. At each time step, the walkers were allowed to move at random to an adjacent voxel. (*B*) The rate at which walkers are absorbed at the vessels wall is $J(t)$. Power-law behavior $J(t) \sim t^{-\alpha}$ appears as a straight line on the $\log(t)$ and $\log(J(t))$ axes. This situation corresponds to clearance following a step change in the intravascular concentration where the mass transfer rate is proportional to the rate at which walkers are absorbed by the vessels. The number of time steps N is related to physical time by $t = Nl^2/2D_mD$ (29) where l is the voxel size ($l \cong 4.7$ μm for normal capillaries), D_m is the diffusivity of the tracer and $D = 3$ is the dimension of the space. We note that these clearance rates from a uniform initial condition are related to the pulse clearance experiments shown in Fig. 2 by $h(t) = -dJ(t)/dt \sim t^{-\alpha-1}$ in the power-law range.

shape of the spaces between vessels, but we observed relatively little dependence on the tissue type in our images. Even though the tumors in our images were only a few millimeters on a side and had developed only small voids we expect diffusion to take an order of magnitude longer than in a normal tissue. The fact that our tracer clearance experiments on 1 mL tumors did not show a transition from power law to exponential decay within the duration of the experiments provides evidence of unperfused voids measuring several millimeters across as would be expected for tumors of this size (14, 15). We can safely predict that diffusion times in clinically relevant tumors will extend over several orders

of magnitude in time. The maximum distance to the nearest vessel is now seen to be an important length scale for extravascular diffusion. However, other features—such as the shape of the spaces in which material diffuses—can influence clearance.

Computational Models of Diffusion Based on Geometric Archetypes. To illustrate how various geometries behave with respect to diffusion and clearance, we ran simulations on several geometrical archetypes covering a range of vascular arrangements observed in vivo (Fig. 4*A*). We are particularly interested in the part of the $n(\delta)$ curve that corresponds to the approximate power-law interval of the clearance curves, roughly $\delta < \delta_{\max}/3$ (recalling that diffusion times scale as $t = \delta^2/D_m$). We have already shown that greater distances are linked to the exponential decay at long times that depends solely on $\delta_{\max}$. Defining λ as the slope of $\log n(\delta)$ vs. $\log \delta$, we see that λ serves as a convexity index—positive for convex shapes and negative for concave shapes (Fig. 4*B*).

Normal capillaries, especially those in a highly structured tissue such as those shown in Fig. 1*A* resemble an array of cylinders with nearly uniform spacing l (Fig. 4*A*, *Upper Left*), similar to the classical Krogh cylinder model used by August Krogh in 1919 to analyze oxygen diffusion near a typical, normal blood vessel (3). Placing the vessels in a random, but uniform distribution (Fig. 4*A*, *Lower Left*) matches the gradual drop in $n(\delta)$ observed for normal vessels better than the Krogh model, but still yields a maximum distance from cell to vessel $\delta_{\max}$ that only modestly exceeds the mean distance between vessels. For both the regular and random patterns we find that convex geometry, typical of the vicinity of a single vessel, dominates. In contrast, tumor vasculature seldom contains repeating patterns, but can show large regions devoid
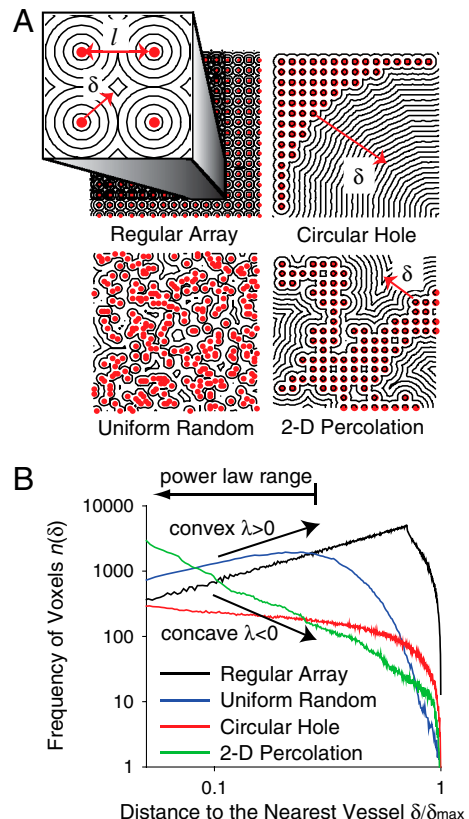
Fig. 4. Interpretation of the convexity index. (*A*) Various arrangements of vessels shown in 2D with contours of δ, distance to the nearest vessel. The mean spacing between adjacent vessels is defined as l. (*B*) Histograms of the number of voxels present at a given distance from the nearest vessel for the arrangements shown in panel *A*.

of functional vessels—that is, there are two distinct length scales δ_{max} and l such that $\delta_{max} \gg l$ where l is the mean distance between vessels in vascularized regions, and δ_{max} is the maximum distance from cell to vessel. For distances between l and δ_{max} we see that $n(\delta)$ decreases ($\lambda < 0$) as expected for a concave geometry. The simplest model for such a region is a circular hole (Fig. 4A, *Upper Right*). An alternative model suitable for irregularly shaped voids may be found in the space around a percolation network (Fig. 4A, *Lower Right*). In an earlier study of 2D images of vessels(16–18), we found that tumor vessels resemble a mesh that has been haphazardly connected so that the resulting network barely maintains connectivity over long distances—the so-called percolation threshold. Much is known about flow of fluid through the interior of such networks from percolation theory that is often used for studying the flow of oil and water through randomly fractured rock. Here our use of the percolation-like geometry is somewhat different. We focus on the diffusion of materials to and from the surface of the network through the space surrounding the network rather than the convective movement of materials within the network. We see in Fig. 4B that $n(\delta)$ calculated for the space around a percolation network shows a gradual, power-law decrease between l and δ_{max} that reflects the existence of avascular voids of many sizes as we often find in tumors (similar results from 3D networks are presented in *SI Discussion, Numerical Simulations for Specific Geometries*). The randomness due to percolation is qualitatively different from that of a uniformly random distribution (Fig. 4A, *Lower Left*)—not only does percolation yield voids on widely different length scales, but it does so while maintaining local connectivity between neighboring vessels, a prerequisite for sustaining flow throughout the network.

Quasi-One-Dimensional Analytical Model of Diffusion in Complex Geometries. We hypothesize that the geometrical exponent λ obtained from 3-D images should be related to the time exponent α observed in the random walk generated clearance curves. Whereas λ drifts somewhat with respect to distance from the vessel for most geometries, a best fit over the range $\delta < \delta_{max}/3$ is sufficiently stable to provide a meaningful, consistent measure of the shape of the space between vessels. We find that the simple relationship $\alpha = (1 - \lambda)/2$ holds well for both real and idealized geometries (Fig. 5 A and B). Further, we show that a quasi-one dimensional diffusion analysis yields exactly this result (derivation *SI Discussion, Analytical Model of Diffusion*, and supporting simulations *SI Discussion, Numerical Simulations for Specific Geometries*).

Here we consider diffusion in 1D, but we account for 3D effects by allowing the area through which diffusion occurs to increase or decrease along a δ-axis measured outward from the blood vessels consistent with our observations that $n(\delta)$ can increase or decrease with distance depending on the geometry of interest. A suitable form of the diffusion equation can be written as

$$D_m \left[\frac{\partial^2 C(\delta,t)}{\partial \delta^2} + \frac{1}{n(\delta)} \frac{dn(\delta)}{d\delta} \frac{\partial C(\delta,t)}{\partial \delta} \right] = \frac{\partial C(\delta,t)}{\partial t},$$

where we consider diffusion of a tracer that does not undergo binding or other chemical transformation. To examine spatial scaling we assume that $n(\delta) \sim \delta^\lambda$ where the well-known cylindrical and spherical coordinates correspond to $\lambda = 1$ and 2, respectively, but where we let λ take on positive or negative, noninteger values as needed. Solving for the flux of material at the vessel wall under appropriate initial and boundary conditions yields exactly $\alpha = (1 - \lambda)/2$ for $\lambda < 1$. Remarkably, our numerical simulations (*SI Discussion, Numerical Simulations for Specific Geometries*) show that this result is robust even when the power-law exponents α and λ are not constant but drift gradually as we have observed, that is, $\alpha(t) \approx (1 - \lambda(\delta))/2$ where $t = \delta^2/D_m$.
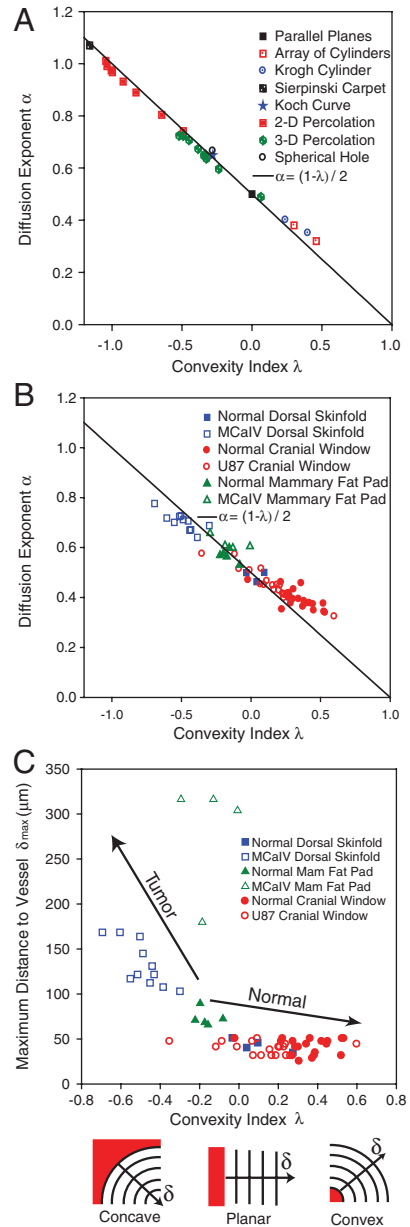
Fig. 5. Geometrical and diffusion parameters in normal and tumor tissues. The convexity indices and the diffusion exponents are calculated from artificial structures (*A*) and from 3D images of several tissue types (*B*). Values of λ are based on the slope of $\log(\delta)$ vs. $\log(n(\delta))$ over the range $\delta < \delta_{max}/3$, whereas α is obtained from the corresponding interval time on the clearance curves $t = \delta^2/D_m$. The equation $\alpha = (1 - \lambda)/2$ is shown to closely predict the relationship in all cases. Panel *C* shows a parametric map for various tissue types of the geometrical measures, δ_{max} and λ, that govern extravascular diffusion. The icons below the convexity axis indicate simple examples of concave, planar, and convex geometries. The array of cylinders represents a regular array of cylindrical vessels on square centers—shown for two ratios of vessel radius to vessel spacing. The classical Krogh cylinder geometry (3) is also shown for two ratios of the vessel diameter to radius of the surrounding tissue cylinder. Ten realizations are shown for 2D (200×200) and 3D ($64 \times 64 \times 64$) percolation clusters at the critical threshold. Results for 6-generation realizations of the Koch curve and Sierpinski carpet are shown. Numerical methods in *SI Discussion, Numerical Simulations for Specific Geometries*. MCaIV is a mammary carcinoma. U87 is a human glioma.

Application of Geometric Measures to Vascular Geometry. We now have two measures of the vascular geometry—δ_{max}, the characteristic length scale that defines the duration of the longest-lasting diffusion processes, and λ, a measure of the shape of the space

between vessels that governs the rate of transport during shorter time intervals when the majority of the material is moved. We propose that, taken together, δ_{max} and λ capture the essential features of extravascular diffusion for any tissue. The parametric map in Fig. 5C shows these measures for normal and tumor tissues grown in three anatomical locations. Not surprisingly, normal tissues show more uniform vascular spacing with a geometry similar to the traditionally used model—a regular array of cylinders. In contrast, most tumors are in the upper left and show more scatter: that is, they have large, irregular unperfused regions that are more concave than is typical for normal tissues. Moreover, our results show that some tumors, such as the early stage U87 glioma in this study, show less abnormality than would be expected in larger tumors. The vascular geometry in tumors typically falls in the range of convexity that is better modeled by spherical holes or percolation networks. We propose that percolation provides the best overall model for tumor vasculature by mimicking the observed architectural heterogeneity as well as the flow heterogeneity as seen in our reexamination of the isolated tumor experiments. We see that δ_{max} and λ can be linked directly to the functional efficiency of the vasculature, are simple enough to be easily conceptualized and can be estimated from information readily available in the clinic such as pathology slides or vascular images.

Discussion

The results of this study should be useful for assessing the delivery of traditional cytotoxic therapy following changes in tumor vasculature following antiangiogenic treatment—a process we have coined "vascular normalization (2, 19). As we learned from preclinical and clinical studies, vascular density alone is not an adequate predictive marker for the success of antiangiogenic therapy used alone or in combination with cytotoxic therapy (20). Drug delivery can be improved by reducing the distance to the nearest vessel and by ensuring that blood flow is sufficiently uniform in the vascular network so that each vessel is well-perfused.

These goals can be achieved by either recruiting blood vessels into previously unperfused regions or by redirecting flow from well-perfused vessels to poorly perfused vessels. Because we can-not expect antiangiogenic drugs to promote significant growth of new vessels, we must consider ways that treatment can restore flow to vessels that may be temporarily unperfused. Antiangiogenic treatment is known to reduce vascular permeability and interstitial fluid pressures within the tumor that may allow unperfused vessels to regain flow (2, 21), thus possibly spanning unperfused voids and reducing δ_{max}. Another approach would be to open compressed vascular pathways using fractionated radiation therapy or cytotoxic agents, which can relieve compressive mechanical stresses on the vessels by reducing the numbers of nearby cancer cells or the density of the extracellular matrix (22, 23). The goal of improving flow in low-flow regions might be achieved by selectively pruning redundant vessels, diverting blood to where it is most needed. Antiangiogenic treatment has been shown to reduce the tortuosity and diameter of tumor vessels (15, 24, 25). Whereas decreased tortuosity has the obvious benefit of shortening the flow pathways, diameter reduction has more subtle implications. Smaller vessels generally offer greater resistance to flow, but bring the promise of tighter regulation and uniformity of flow throughout the network. Our results provide a theoretical underpinning for how vascular normalization by antiangiogenic treatment, which was originally intended to starve the tumor of nutrients, can improve delivery of blood-borne agents (2, 19).

Materials and Methods

The Doppler optical frequency domain and multiphoton imaging methods used to image the vasculature are described in *SI Materials and Methods*. Analytical derivations and the methods used for numerical simulations are detailed in *SI Discussion, Analytical Model of Diffusion* and *SI Discussion, Numerical Simulations for Specific Geometries*, respectively.

1. Endrich B, Reinhold HS, Gross JF, Intaglietta M (1979) Tissue perfusion inhomogeneity during early tumor growth in rats. *J Natl Cancer Inst* 62:387–395.
2. Jain RK (2005) Normalization of tumor vasculature: An emerging concept in antiangiogenic therapy. *Science* 307:58–62.
3. Krogh A (1919) The number and distribution of capillaries in muscles with calculations of the oxygen pressure head necessary for supplying the tissue. *J Physiol* 52:409–415.
4. West GB, Brown JH, Enquist BJ (1997) A general model for the origin of allometric scaling laws in biology. *Science* 276:122–126.
5. West GB, Brown JH, Enquist BJ (1999) The fourth dimension of life: Fractal geometry and allometric scaling of organisms. *Science* 284:1677–1679.
6. Jain RK, Baxter LT (1988) Mechanisms of heterogeneous distribution of monoclonal antibodies and other macromolecules in tumors: Significance of elevated interstitial pressure. *Cancer Res* 48:7022–7032.
7. Helmlinger G, Yuan F, Dellian M, Jain RK (1997) Interstitial pH and pO2 gradients in solid tumors in vivo: High-resolution measurements reveal a lack of correlation. *Nat Med* 3:177–182.
8. Eskey CJ, Wolmark N, McDowell CL, Domach MM, Jain RK (1994) Residence time distributions of various tracers in tumors: Implications for drug delivery and blood flow measurement. *J Natl Cancer Inst* 86:293–299.
9. Bassingthwaighte JB, Beard D (1995) Fractal ^{15}O-labeled water washout from the heart. *Circ Res* 77:1212–1221.
10. Leunig M, et al. (1992) Angiogenesis, microvascular architecture, microhemodynamics, and interstitial fluid pressure during early growth of human adenocarcinoma LS174T in SCID mice. *Cancer Res* 52:6553–6560.
11. Yuan F, et al. (1994) Vascular permeability and microcirculation of gliomas and mammary carcinomas transplanted in rat and mouse cranial windows. *Cancer Res* 54:4564–4568.
12. Pries AR, Hopfner M, le Nobel F, Dewhirst MW, Secomb TW (2010) The shunt problem: Control of functional shunting in normal and tumour vasculature. *Nat Rev Cancer* 10:587–593.
13. Risser L, et al. (2007) From homogeneous to fractal normal and tumorous microvascular networks in the brain. *J Cereb Blood F Met* 27:293–303.
14. Gaustad J-V, Benjaminsen IC, Ruud E-BM, Rofstad EK (2007) Dynamic contrast-enhanced magnetic resonance imaging of human melanoma xenografts with necrotic regions. *J Magn Reson Imaging* 26:133–143.
15. Batchelor TT, et al. (2007) AZD2171, a pan-VEGF receptor tyrosine kinase inhibitor, normalizes tumor vasculature and alleviates edema in glioblastoma patients. *Cancer Cell* 11:83–95.
16. Gazit Y, Berk DA, Leunig M, Baxter LT, Jain RK (1995) Scale-invariant behavior and vascular network formation in normal and tumor tissue. *Phys Rev Lett* 75:2428–2431.
17. Gazit Y, et al. (1997) Fractal characteristics of tumor vascular architecture during tumor growth and regression. *Microcirculation* 4:395–402.
18. Baish JW, Jain RK (2000) Fractals and cancer. *Cancer Res* 60:3683–3688.
19. Jain RK (2001) Normalizing tumor vasculature with anti-angiogenic therapy: A new paradigm for combination therapy. *Nat Med* 7:987–989.
20. Jain RK, et al. (2009) Biomarkers of response and resistance to antiangiogenic therapy. *Nat Rev Clin Oncol* 6:327–338.
21. Jain RK, Tong RT, Munn LL (2007) Effect of vascular normalization by antiangiogenic therapy on interstitial hypertension, peritumor edema, and lymphatic metastasis: Insights from a mathematical model. *Cancer Res* 67:2729–2735.
22. Olive KP, et al. (2009) Inhibition of hedgehog signaling enhances delivery of chemotherapy in a mouse model of pancreatic cancer. *Science* 324:1457–1461.
23. Padera TP, et al. (2004) Cancer cells compress intratumor vessels. *Nature* 427:695.
24. Tong RT, et al. (2004) Vascular normalization by vascular endothelial growth factor receptor 2 blockade induces a pressure gradient across the vasculature and improves drug penetration in tumors. *Cancer Res* 64:3731–3736.
25. Winkler F, et al. (2004) Kinetics of vascular normalization by VEGFR2 blockade governs brain tumor response to radiation: Role of oxygenation, angiopoietin-1, and matrix metal loproteinases. *Cancer Cell* 6:553–563.
26. Brown EB, et al. (2001) In vivo measurement of gene expression, angiogenesis, and physiological function in tumors using multiphoton laser scanning microscopy. *Nat Med* 7:864–868.
27. Jain RK, Munn LL, Fukumura D (2002) Dissecting tumour pathophysiology using intravital microscopy. *Nat Rev Cancer* 2:266–276.
28. Vakoc BJ, et al. (2009) Three-dimensional microscopy of vascular networks, lymphatics, cell viability, and tissue microenvironment in vivo using optical frequency domain imaging. *Nat Med* 15:1219–1224.
29. Ben-Avraham D, Havlin S (2000) *Diffusion and Reactions in Fractals and Disordered Systems* (Cambridge University Press, Cambridge, UK).

ENGINEERING

MEDICAL SCIENCES